Polypeptide-Based Nanocomposite: Structure and Properties of Poly(L-lysine)/Na^+-Montmorillonite*

VAHIK KRIKORIAN[1,2], MARY KURIAN[1], MARY E. GALVIN[1], ANDREW P. NOWAK[3], TIMOTHY J. DEMING,[3] DARRIN J. POCHAN[1,2]

[1]Department of Materials Science and Engineering, University of Delaware, Newark, Delaware 19716

[2]Delaware Biotechnology Institute, University of Delaware, Newark, Delaware 19716

[3]Department of Materials and Chemistry, University of California, Santa Barbara, California 93106

Received 17 May 2002; revised 1 August 2002; accepted 21 August 2002

ABSTRACT: The feasibility of constructing polymer/clay nanocomposites with polypeptides as the matrix material is shown. Cationic poly-L-lysine · HBr (PLL) was reinforced by sodium montmorillonite clay. The PLL/clay nanocomposites were made via the solution-intercalation film-casting technique. X-ray diffraction and transmission electron microscopy data indicated that montmorillonite layers intercalated with PLL chains coexist with exfoliated layers over a wide range of relative PLL/clay compositions. Differential scanning calorimetry suggests that the presence of clay suppresses crystal formation in PLL relative to the neat polypeptide and slightly decreases the PLL melting temperature. Despite lower crystallinity, dynamic mechanical analysis revealed a significant increase in the storage modulus of PLL with an increase in clay loading producing storage modulus magnitudes on par with traditional engineering thermoplastics. © 2002 Wiley Periodicals, Inc. J Polym Sci Part B: Polym Phys 40: 2579–2586, 2002

Keywords: clay; nanocomposites; morphology; peptides; biomaterials; biopolymers

INTRODUCTION

Natural and synthetic clays have received much attention as inorganic reinforcement materials in the field of nanocomposites because of their small particle size, nanometer level dispersion, good intercalation properties, mechanical strength, and large surface area for adsorption of organic molecules.[1,2] Incorporation of small amounts of layered silicates in a suitable polymer matrix results in significant improvements in the mechanical,[3] thermal stability,[4–6] gas barrier,[7,8] and flame-retardant[9] properties of the nanocomposite versus the pure organic phase. Sodium montmorillonite (MMT) is a hydrophilic, mica-type, 2:1 phyllosilicate that forms stable suspensions in water,[10] making it ideal for dispersion into water-soluble polymers such as poly(vinyl alcohol),[10,11] poly(ethylene oxide),[12,13] poly(acrylic acid),[14] or poly(*N*-vinyl pyrrolidone).[15]

Numerous studies have focused on micro- and nanocomposites with biocompatible and biodegradable polymers.[16–19] Several motivations drive the search for biodegradable and biocompatible polymers as matrices for composites. Producing engineering and commodity materials out of environmentally biodegradable polymers [such as

*Contribution from the March 2002 Meeting of the American Physical Society—Division of Polymer Physics, Indianapolis, Indiana

Correspondence to: D. J. Pochan (E-mail: pochan@udel.edu)

Journal of Polymer Science: Part B: Polymer Physics, Vol. 40, 2579–2586 (2002)

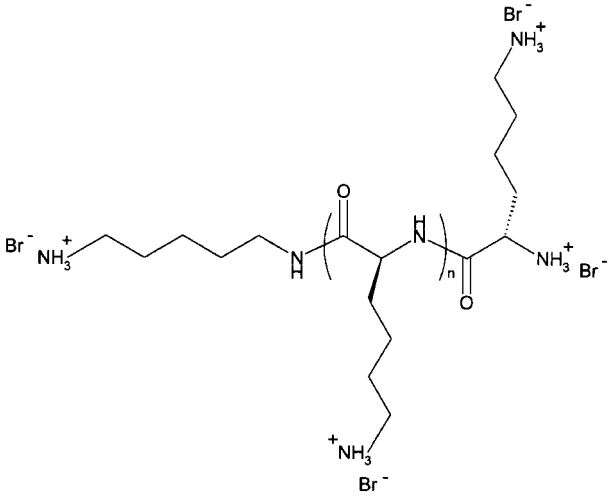

Figure 1. Chemical structure of PLL.

article coating, textile sizing, and flexible water-soluble packaging films produced from poly(vinyl alcohol)[20]] results in materials with "green" degradation pathways. Polymers with *in vivo* biodegradable pathways can be used in composites for advanced biomaterials such as sutures produced from poly(lactide-*co*-glycolide)-based polymers,[21] drug-delivery matrices,[22] and so forth within the body. Composites with inherent biocompatibility with living tissues create the potential for use as load-bearing implants in orthopedic surgery, blood vessels, and other replacement biomaterials within the body.[23]

Although nanocomposites have been produced with an extensive, disparate array of synthetic polymers, to our knowledge the effect of MMT incorporation on matrices of biological origin in general, and on polypeptides in particular, has not been investigated. This study specifically investigates the feasibility of making a new class of nanocomposites in which the matrix is a polypeptide. The candidate polypeptide used in this study is the homopolymer poly-L-lysine · HBr (PLL). A cationic polymer at neutral pH, PLL is ubiquitous in biotechnology labs as a cell-adhesion agent for cell-culturing experiments in plates and on other solid substrates.[24] We envisioned the cationic primary amine groups of the lysine amino acid side chains (Fig. 1) should interact with the negatively charged silicate layers of MMT resulting in nanometer-range dispersion and nanocomposite formation. The general use of polypeptides as nanocomposite matrices introduces intriguing possibilities for the design and construction of versatile, advanced materials. In addition to having improved mechanical, barrier, and thermal properties, nanocomposites produced with polypeptide matrices could have *a priori* designed, inherent biological functionality (such as biocompatibility, antimicrobial properties, or specific cell-targeting capabilities) and morphological control via secondary structure-phase transitions of the polypeptide matrix molecules.

For this investigation, nanocomposites of PLL/MMT with varying polypeptide-to-clay compositions were prepared. Nanocomposite formation and morphology were monitored via X-ray diffraction (XRD) and transmission electron microscopy (TEM). Thermal properties of the nanocomposites and the effects of clay incorporation on the extent of PLL crystallization were measured with differential scanning calorimetry (DSC) and thermogravimetric analysis (TGA). Dynamic viscoelastic properties of the nanocomposites were directly measured with dynamic mechanical analysis (DMA). The results of these initial studies presented herein reveal successful nanocomposite formation with PLL and MMT, resulting in strong peptide-based materials.

EXPERIMENTAL

Materials

PLL with a number-average molecular weight of 2.7×10^5 g/mol and a polydispersity of 1.28 was prepared according to published procedures.[25] Natural clay, Wyoming Na+-montmorillonite (Swy-2) with a cation-exchange capacity of 76.4 meq/100 g was obtained from the Clay Minerals Repository at the University of Missouri (Columbia, MO).

Purification of MMT

Approximately 15 g of MMT were gradually added into deionized (DI) water and stirred overnight. The solution was subsequently kept static allowing heavy impurities to sediment. Then the separated clean clay solution was decanted from the impurities. This process was repeated two times resulting in a pure clay solution. The solution was centrifuged to separate the clean clay from the DI water. The clay was subsequently dried in a vacuum oven for 48 h at 60 °C and then ground into a powder with a mortar and pestle.

Nanocomposite Preparation

Four different compositions of PLL/MMT nanocomposites were prepared (2, 5, 10, and 15 wt %

MMT in PLL) with the solution-intercalation film-casting technique. For each composition, 100 mg of PLL were dissolved in 250 mL of DI water in a 500-mL beaker. Clay solutions (<0.1 wt %) were obtained by suspending a measured amount of clay in a separate 500-mL beaker containing 250 mL of DI water. The polypeptide and clay solutions were stirred separately overnight and then mixed together and stirred again for 12 h. The water was evaporated in a rotating evaporator under vacuum at 50 °C. Because PLL sticks firmly to bare glass, a poly(tetrafluoroethylene) coated round-bottom flask was used to evaporate the water. After 15 min the highly concentrated solution was poured into a silicon rubber mold, and the remaining water was allowed to evaporate. The solid nanocomposite films, several hundred microns in thickness, were further dried in a vacuum oven for 48 h at 60 °C and subsequently cooled to ambient temperature under vacuum. The final nanocomposite films were strong, tear resistant materials that were also optically clear.

CHARACTERIZATION

X-ray Diffraction

XRD experiments were performed in transmission mode on a pinhole-collimated camera equipped with a Rigaku copper target rotating anode (Cu Kα radiation λ = 1.54 Å) operating at 3.6 kW. Data were collected with a two-dimensional Bruker charged coupling device detector. The isotropically scattered data were azimuthally integrated into one-dimensional profiles of intensity versus scattering angle, 2θ. The samples were scanned several times and rotated/translated between scans to ensure no orientation existed in the samples; isotropic scattering resulted in all samples.

TEM

TEM bright field imaging was performed with a JEOL 2000FX microscope with 100-kV accelerating voltage. To preserve the *in situ* nanocomposite structure, samples were microtomed into ultrathin slices (<100 nm thickness) without embedding, with a diamond knife. Because of their tough, glassy character [glass-transition temperature (T_g) ~56 °C as observed via DMA; see results and discussion section), samples were microtomed at room temperature.

Thermal Analysis

The nanocomposite thermal behavior was measured with a TA Instruments DSC and TGA model Q100 series instrument. Experiments were performed under constant nitrogen flow with a heating rate of 10 °C/min. In an attempt to precisely observe the effect of clay incorporation on PLL crystallinity, the DSC samples were weighed such that all of the samples had an identical PLL content. The sample weight was maintained at low levels (1–2 mg) for all measurements to minimize any possible thermal lag during the scans. Temperature and heat of fusion were calibrated with an indium standard.

Mechanical Analysis

DMA experiments were performed on a TA Instruments 2980 DMA apparatus equipped with a film-tension clamp. The instrument was programmed to measure E' and E'' over the range of 0–100 °C at 2 °C/min heating rate and 1 Hz constant frequency. Calibrations for force, mass position, and temperature were made in accordance with TA Instruments procedures. The specimen films were cut with length-to-width ratios >6 to guarantee uniform strain in the films under tension. The applied strain (0.02–0.05%) was well within the linear viscoelastic region of the samples, and the collected data were reproducible. The T_g of the samples was defined as the temperature where tan δ was a maximum.

RESULTS AND DISCUSSION

Morphology

XRD patterns of neat PLL; neat MMT; and 2, 5, 10, and 15 wt % MMT in PLL nanocomposites are given in Figure 2. The diffraction pattern for pure PLL consists of two peaks because of the semicrystalline structure of PLL. These two peaks are present in all of the nanocomposite X-ray patterns, indicating that the added clay particles do not completely disrupt crystallization or alter the crystal structure within the PLL matrix. Conversely, the characteristic peak of pristine MMT that corresponds to the interlayer spacing, $d(001)$ = 10.46 Å, of the constituent silica layers is completely eliminated in all of the nanocomposites, indicating either complete intercalation or exfoliation of all the pure silica layers.

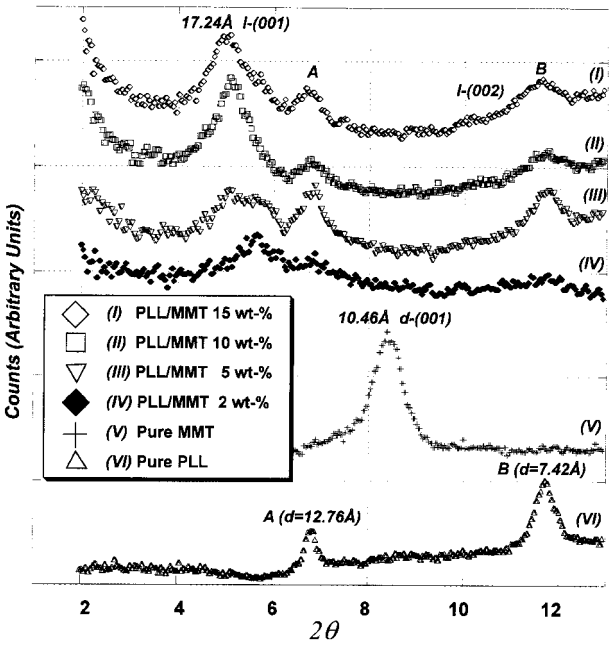

Figure 2. Comparison of XRD patterns for different compositions of neat PLL; neat MMT; and 2, 5, 10, and 15 wt % MMT in PLL nanocomposites. The two primary crystal diffraction peaks of neat PLL corresponding to spacings of 12.76 and 7.42 Å are labeled A and B, respectively. The first-order reflection originating from the interplatelet long spacing of pure MMT is labeled *d*-(001). The first-order reflection originating from the interplatelet long spacing after PLL intercalation is labeled I-(001), and the second-order reflection is I-(002).

Comparing the neat MMT diffraction pattern with the high-clay-content (10 and 15 wt %) nanocomposite samples, one observes a new peak at 17.24 Å (I-001). This peak corresponds to the clay interlayer galleries intercalated with PLL. The spacing was regular enough to produce weak second-order reflections (I-002) also visible in Figure 2. In the lower clay content samples (2 and 5 wt %), the magnitude of gallery increase via intercalation of PLL was lower than that observed in the higher clay loadings. Interestingly, at high clay content the silicate layers seem to have expanded farther apart than in the dilute samples. This intermediate spacing between pure MMT and the high clay-loading nanocomposites was reproducible in different nanocomposite batches of the same composition. Importantly, all of the intercalated scattering peaks are quite broad indicating a large population of intercalated intergallery spacings.

Typical TEM micrographs of the 10 wt % nanocomposite are illustrated in Figure 3(a,b). Both images reveal the coexistence of disordered, exfoliated sheets of MMT layers (I) and intercalated tactoids (II). In addition, many silicate layers are normal to the electron beam and appear as large, dark areas (III), masking whether the platelet is exfoliated or part of an intercalated tactoid. The intercalated tactoids in the TEM data are what produce the XRD pattern in Figure 2, whereas the disordered, exfoliated MMT regions have no periodic stacking and consequently have no characteristic peaks in the diffraction patterns.[1,26] The measured interlayer spacings between adjacent clay layers of intercalated tactoids from TEM

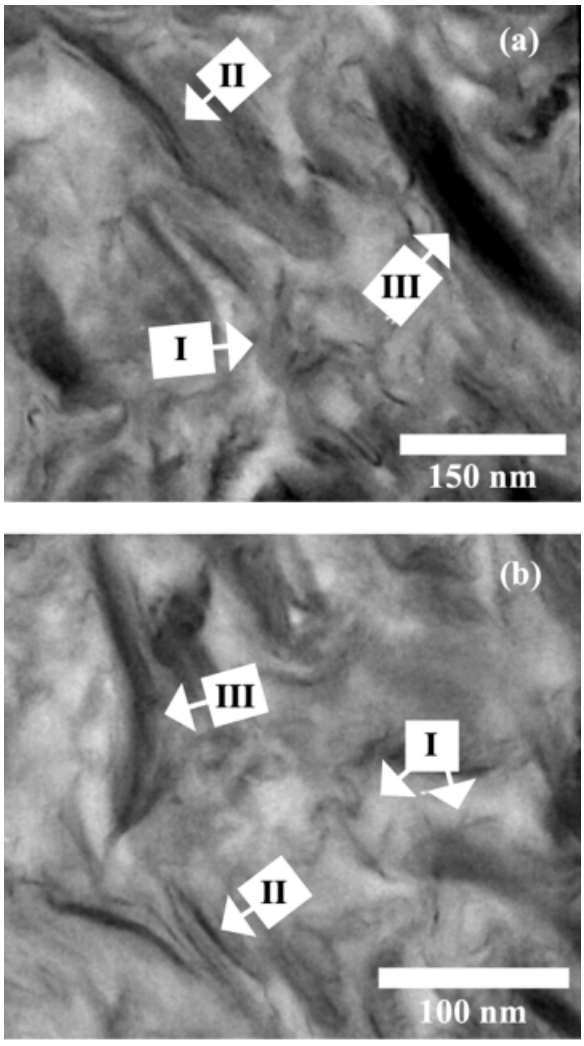

Figure 3. (a) and (b) TEM bright field images of semicrystalline PLL/MMT (10 wt % MMT) nanocomposite showing a mixture of intercalated clay tactoids (I), exfoliated clay platelets (II), and clay platelets parallel to the material cross section/normal to the electron beam (III).

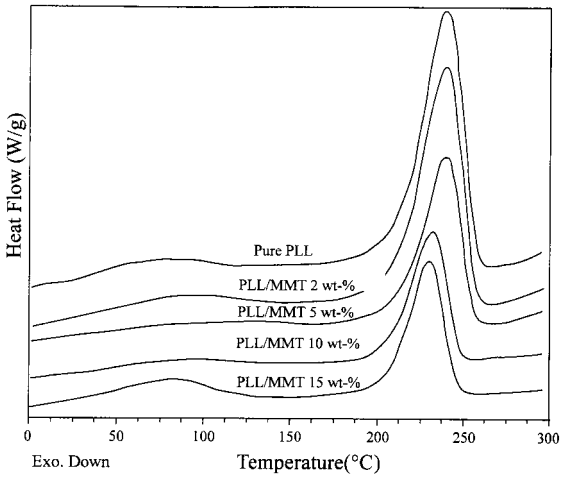

Figure 4. Comparison of DSC thermographs for all relative PLL to MMT compositions studied (graphs are offset vertically for clarity).

bright field images are consistent with the XRD data. Similar exfoliated/intercalated mixed morphologies are observed in the three other nanocomposite formulations and are not shown. The micrographs emphasize the good nano- to microscale dispersion of the MMT filler in the PLL matrix.

Thermal Characterization

DSC thermographs of the samples with different clay compositions versus pure PLL are portrayed in Figure 4. By integrating the area under the endothermic region of the curves, heat of fusion for each of the nanocomposite compositions was calculated. The results are given in Figure 5(a). The highest heat of fusion (i.e., the highest percentage of PLL crystallinity) was observed in pure PLL. As the clay content increased, the heat of fusion dropped indicating that the inorganic clay particles hinder the overall extent of PLL crystallization from solution.

The melting point (T_m) of the samples was evaluated from the position of the maximum in the endothermic peaks of DSC thermographs [Fig. 5(b)]. The T_m of the nanocomposites slightly decreased with an increasing MMT content. Both a decrease in the amount of crystallinity and a decrease in T_m have been observed in poly(ϵ-caprolactone) clay blends[18] and was attributed to a decrease in the crystallite dimension as a result of adding clay to the pure polymer. Likewise, the clay particles may act as nucleants for PLL crystallization from solution, thereby increasing the number of crystal embryos and consequently lowering the size of PLL crystallites within the final nanocomposite and slightly lowering the PLL melting point. Thermal glass transitions seem to occur around 50 °C, although the transitions are somewhat ambiguous. A much clearer indication of T_g in pure PLL and PLL/MMT nanocomposites was observed via strong tan δ maxima in the DMA measurements reported subsequently.

TGA of pure PLL and the 5 and 15 wt % MMT in PLL nanocomposite compositions are depicted in Figure 6. The 2 and 10 wt % MMT composites exhibited very similar behavior to the 5 and 15 wt % nanocomposites but are not shown. Three specimens for TGA were cut from different parts of

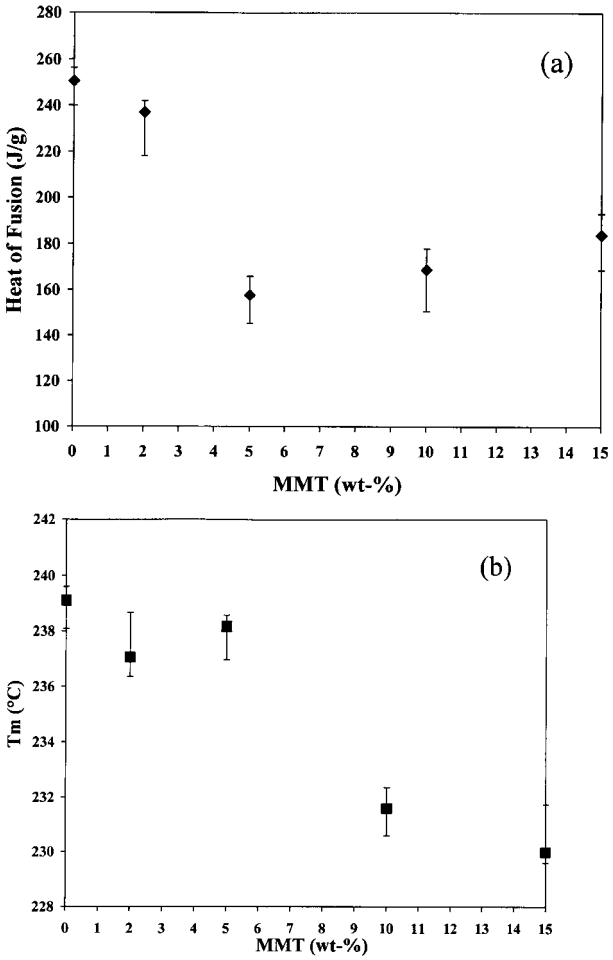

Figure 5. (a) Heat of fusion and (b) melting point variations of PLL/MMT nanocomposites with respect to clay composition. In both (a) and (b), the results of three measurements are exhibited by the data point representing the middle observed value, and the error bars represent the total spread of the three measurements.

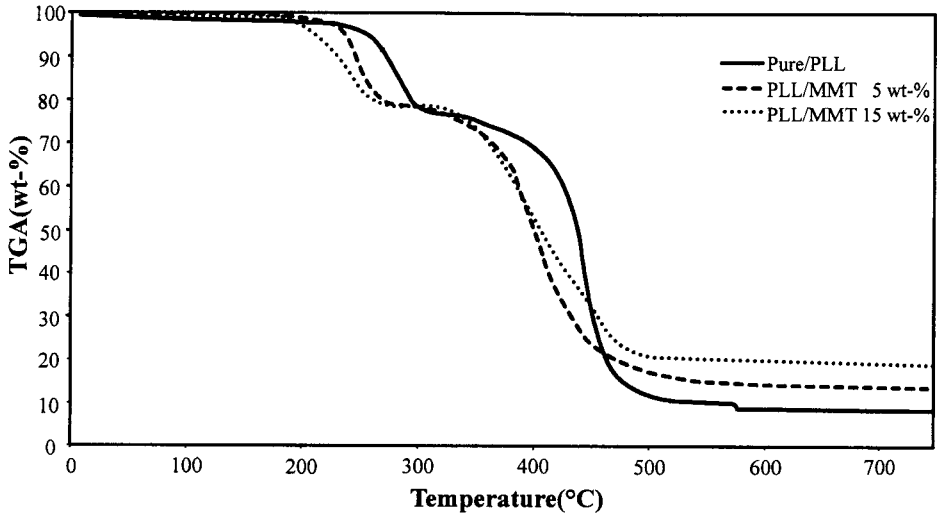

Figure 6. PLL weight loss from TGA scans for 5 and 15 wt % MMT in PLL nanocomposites and pure PLL.

each sample composition. The TGA experiments were performed on each specimen resulting in identical degradation curves for all three specimens from the same composition. Initially, the weight of ash produced by a known amount of pure PLL was directly measured. By first measuring the amount of char as a percentage of solids remaining from an original known amount of pure PLL, one can subsequently calculate the amount of polymer char because of known original amounts of PLL versus MMT in all of the nanocomposites. As indicated by the TGA curve reproducibility between specimens cut from the same sample and the small disparity between clay contents calculated from final ash content versus original nanocomposite formulation (difference in MMT content <0.1 wt %), the clay was dispersed homogeneously throughout the matrix. This conclusion is also supported by the TEM micrographs in Figure 3(a,b).

All of the samples exhibit similar behavior—a slight weight loss around ~100 °C corresponding to water loss, an approximately 20% weight loss subsequent to melting, and a final significant weight loss down to a final ash content above 300 °C. As indicated by the initial weight loss, the equilibrium water levels of the nanocomposites were $\ll 1.0$ wt %, whereas the water content of the pure PLL was ~2.0 wt %. The two large shoulders in the thermal-degradation curves of all the samples, which correspond to degradation of the material in two steps, have been reported for other types of matrices such as polyaniline[27] and poly(ethylene oxide).[28] In the case of polyaniline,[29,30] the degradation at lower temperature was attributed to evaporation of acid dopant, and the second transition was attributed to the degradation of the polymer backbone. The bimodal degradation of PLL and the lower PLL degradation temperature with clay loading observed in Figure 6 requires further investigation to identify specific degradation mechanisms, and work is now underway.

Mechanical Properties

Figure 7(a,b) shows the temperature dependence of the storage tensile modulus, E', and tan δ of the pure PLL, 10 and 15 wt % clay nanocomposites. A clear transition exists between 40 and 60 °C in all of the samples. The E' of the 10 and 15 wt % MMT nanocomposites is higher than pure PLL over the entire range of temperature. Above 60 °C the behavior of the samples becomes matrix dependent, and the difference between the storage moduli of the 10 and 15 wt % MMT content samples decreases. However, the magnitude of storage moduli in the nanocomposites is still higher than that observed in pure PLL. The tan δ curves in Figure 7(b) suggest a clear maximum at 56 °C, which is defined as the T_g of PLL. The temperature at which the tan δ is a maximum does not change significantly by adding clay. Although the DSC experiments (Fig. 4) provided ambiguous T_g results, DMA provided an unambiguous observation of T_g. In addition, because the peak of tan δ

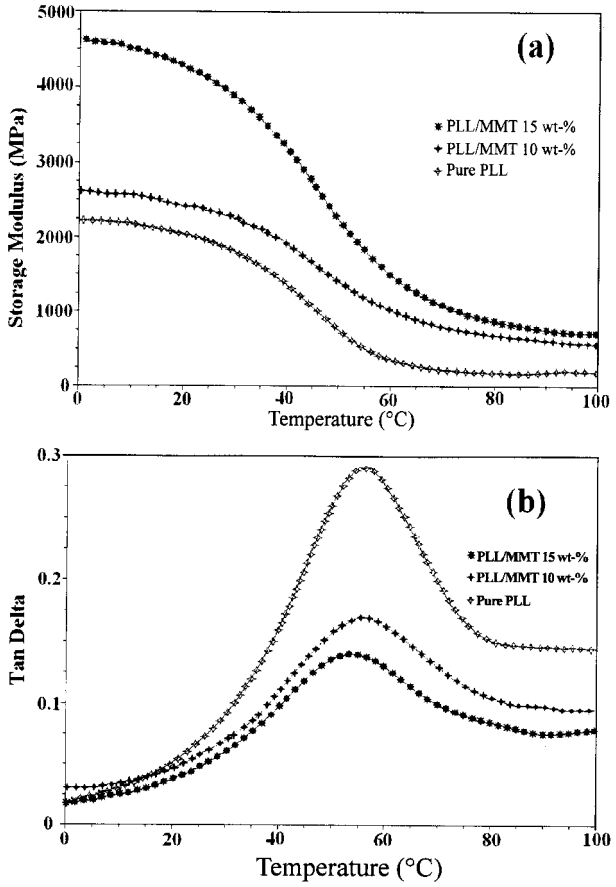

Figure 7. Dynamic viscoelastic behavior of PLL/MMT nanocomposites: (a) storage modulus, E', and (b) tan δ. The average of three measurements is plotted for all samples. The average standard deviation of the DMA data is ±205, ±97, and ±110 MPa for the 15, 10, and 0 wt % (pure PLL) MMT samples, respectively. The standard deviations in temperature of the maximum tan δ are ±2.1, ±3.5, and ±1.3 °C for the 15, 10, and 0 wt % (pure PLL) MMT samples, respectively. The uncertainties are not plotted in the data for the sake of clarity.

decreased by adding clay, it can be concluded that damping properties of the samples decreased by increasing the MMT loading.

It is useful to compare the observed PLL/MMT nanocomposite mechanical behavior with the behavior of thoroughly examined polymer/inorganic composite matrices. Previously, Nazhat and coworkers[31,32] prepared conventional microscale composites with biodegradable poly-D,L-lactic acid/hydroxyapatite (HA) and high-density polyethylene/HA. The viscoelastic behavior of the preceding two literature examples of biomaterial composite systems at 20 and 37 °C, as characterized by DMA, are listed in Table 1 for comparison with the 10 and 15 wt % MMT in PLL nanocomposite results. The PLL-based nanocomposites exhibit mechanical properties commensurate with the literature examples of materials aimed at *in vivo* bone regeneration and load-bearing implants, highlighting the intriguing possibilities of polypeptide-based nanocomposites for biomaterial technology.

CONCLUSIONS

We have investigated the structural, thermal, and mechanical properties of PLL/MMT nanocomposites formed by clay intercalation/exfoliation in aqueous solution. According to TEM and XRD studies, a coexistence of exfoliated and intercalated clay exists in the final nanocomposites that reveals a robust tendency of PLL to disperse on a nanometer length scale. Thermal studies revealed PLL to be a semicrystalline material when cast from solution and that its crystallinity is suppressed with the addition of MMT filler to form nanocomposites. The PLL/MMT nanocomposites were thermally stable up to the melting point of PLL, after which the materials degrade via a bimodal mechanism. Importantly, the mechanical properties of semicrystalline PLL and PLL/MMT nanocomposites are similar to investigated biodegradable polymers and engineering thermoplastics used in composites for biomedical and commodity materials applications. Additional attributes of the polypeptide matrix, such as optical transparency and easy functionalization with additional bioactive peptide sequences, make these nanocomposites promising candi-

Table 1. Comparison of Tensile Storage Modulus of PLL/MMT (10 and 15 wt % MMT) Nanocomposites with PDLLA and PDLLA + HA (from Nazhat et al.[31]), PE, and PE + HA (from Nazhat et al.[32])

Material	E' at 20 °C (GPa)	E' at 37 °C (GPa)
PDLLA[31]	3.3	3.2
PDLLA + HA[31]	6.4	6.2
PE[32]	1.4	1.1
PE + HA[32]	2.6	2.1
Pure PLL	2.1	1.5
PLL/MMT 10 wt %	2.5	2.05
PLL/MMT 15 wt %	4.3	3.5

dates for both traditional materials and advanced biomaterials applications. Furthermore, the conformation of PLL in solution is strongly dependent on solution conditions such as temperature, pH, salt concentration, and alcohol content,[33–35] which provides the opportunity to study the effect of PLL secondary structure/conformation on the intercalated spacings and overall nanocomposite morphology formed.

V. Krikorian and D. J. Pochan are grateful to the thermal-analysis lab at the Center of Composite Materials (UD-CCM) for their generous donation of the thermal-analysis instrument time. The authors would like to acknowledge the ACS-PRF (Award Number 35577-G7) for partial funding of this work.

REFERENCES AND NOTES

1. Giannelis, E. P.; Krishnamoorti, R.; Manias, E. Adv Polym Sci 1999, 138, 107–147.
2. Pinnavaia, T. J. Science 1983, 220, 365–371.
3. Kojima, Y.; Usuki, A.; Kawasumi, M.; Okada, A.; Fukushima, Y.; Kurauchi, T.; Kamigaito, O. J Mater Res 1993, 6, 1185–1189.
4. Burnside, S. D.; Giannelis, E. P. Chem Mater 1995, 7, 1597–1600.
5. Lee, D. C.; Jang, L. W. J Appl Polym Sci 1998, 68, 1997–2005.
6. Noh, M. W.; Lee, D. C. Polym Bull 1999, 42, 619–626.
7. Yano, K.; Usuki, A.; Okada, A. J Polym Sci Part A: Polym Chem 1997, 35, 2289–2294.
8. Lan, T.; Kaviratna, P. D.; Pinnavaia, T. J. Chem Mater 1994, 6, 573–575.
9. Gilman, J. W. Appl Clay Sci 1999, 15, 31–49.
10. Ogata, N.; Kawakage, S.; Ogihara, T. Appl Polym Sci 1997, 66, 573–581.
11. Strawhecker, K. E.; Manias, E. Chem Mater 2000, 12, 2943–2949.
12. Zhao, X.; Urano, K.; Ogasawara, S. Colloid Polym Sci 1989, 267, 899–906.
13. Ogata, N.; Kawakage, S.; Ogihara, T. Polymer 1997, 38, 5115–5118.
14. Billingham, J.; Breen, C.; Yarwood, J. Vibr Spectrosc 1997, 14, 19–34.
15. Levy, R.; Francis, C. W. Colloid Interface Sci 1975, 50, 442–450.
16. Bjork, N.; Ekstrand, K.; Ruyter, I. E. Biomaterials 1986, 7, 73–75.
17. Messersmith, P. B.; Giannelis, E. P. J Polym Sci Part A: Polym Chem 1995, 33, 1047–1057.
18. Jimenez, G.; Ogata, N.; Kawai, H.; Ogihara, T. J Appl Polym Sci 1997, 64, 2211–2220.
19. Ogata, N.; Jimenez, G.; Kawai, H.; Ogihara, T. J Polym Sci Part B: Polym Phys 1997, 35, 389–396.
20. Bassner, S. L.; Klingenberg, E. H. Am Ceram Soc Bull 1998, 77, 71–75.
21. Jain, R. A. Biomaterials 2000, 21, 2475–2490.
22. Kamath, K. R.; Park, K. Drug Delivery Rev 1993, 11, 59–84.
23. Ramakrishna, S.; Mayer, J.; Wintermantel, E.; Leong, K. W. Compos Sci Technol 2001, 61, 1189–1224.
24. Jacobson, B. S.; Branton, D. Science 1977, 195, 302–304.
25. Deming, T. J. Macromolecules 1999, 32, 4500–4502.
26. Alexandre, M.; Dubois, P. Mater Sci Eng 2000, 28, 1–63.
27. Lee, D.; Char, K. Polym Degrad Stab 2002, 75, 555–560.
28. Bujdak, J.; Hackett, E.; Giannelis, E. P. Chem Mater 2000, 12, 2168–2174.
29. Pielichowski, K. Solid State Ionics 1997, 104, 123–132.
30. Wei, Y.; Hsueh, K. F. J Polym Sci Part A: Polym Chem 1989, 27, 4351–4363.
31. Nazhat, S. N.; Kellomaki, M.; Tormala, P.; Tanner, K. E.; Bonfield, W. J Biomed Mater Res 2001, 58, 335–343.
32. Nazhat, S. N.; Joseph, R.; Wang, M.; Smith, R.; Tanner, K. E.; Bonfield, W. J Mater Sci: Mater Med 2000, 10, 621–628.
33. Yu, T. J.; Lippert, J. L.; Peticola, W. L. Biopolymers 1973, 9, 2161–2176.
34. Epand, R. F.; Scheraga, H. A. Biopolymers 1968, 6, 1383–1386.
35. Satoh, M.; Hirose, T. Polymer 1993, 34, 4762–4766.